FUSION OF MULTIPLE FEATURES FOR LAND COVER CLASSIFICATION

Wenzhi Liao[1], *Hongyan Zhang*[1,2], *Jie Li*[1,3], *Shaoguang Huang*[1], *Rui Wang*[1,4], *Renbo Luo*[1,5], *Xingzhe Xie*[1]
Aleksandra Pižurica[1]

[1]Ghent University-TELIN-IPI-iMinds, Sint-Pietersnieuwstraat 41, B-9000 Ghent, Belgium
[2]The State Key Laboratory of Information Engineering in Surveying, Mapping, and Remote Sensing, Wuhan University, China
[3]School of Electronics & Information Engineering, Xi'an Jiaotong University, Xi'an 710049, China
[4]Sichuan Provincial Key Laboratory of Information Coding and Transmission, Southwest Jiaotong University, Chengdu 610031, China
[5]School of Automation Science and Engineering, South China University of Technology, 510640 Guangzhou, China
Email: {wliao, hozhang, jiejli, shhuang, ruiwan, reluo, Xingzhe.Xie and sanja}@telin.ugent.be

ABSTRACT

Hyperspectral imagery contains a wealth of spectral and spatial information that can improve target detection and recognition performance. Existing feature extraction methods cannot fully utilize both the spectral and spatial information. Data fusion by simply stacking different feature sources together does not work well either, as it does not take into account the differences between feature sources. In this paper, we present our recent graph-based approach for fusing multiple feature sources for land cover classification. Our approach takes into account the properties of different data sources, and makes full advantage of different feature sources through the fusion graph. Experimental results in the classification of real hyperspectral images are very encouraging.

Index Terms— Hyperspectral images, remote sensing, classification, data fusion

1. INTRODUCTION

Recent advances in sensors technology have led to an increased availability of hyperspectral (HS) data at very high both spatial and spectral resolutions. Many approaches have been developed to exploit the spectral and the spatial information of hyperspectral imagery for classification. Some of these approaches focus on increasing the spectral discrimination through dimension reduction [1]. Others explore the spatial information of HS data through morphological features [2–5].

A limitation of the above approaches is that they rely mainly on a single type of features (spectral or geometrical features) and do not fully utilize the wealth of information available in the HS data. The spatial information, once combined with the spectral information, can contribute to a more comprehensive interpretation of objects on the ground. For example, spectral signatures cannot differentiate between objects made of the same material (e.g. roofs and roads made with the same asphalt), while they can often be easily distinguished by their geometry. On the other hand, spatial features alone may fail to discriminate between objects that are quite different in nature (e.g. grass field, parking or a swimming pool), if their shape and size are similar. Many approaches have been developed to fuse the spectral and spatial information for the classification of remote sensing data [6, 8–11]. Some of these approaches employ the so-called composite kernel methods [6, 7] or their generalization [9]. Others define spatial information through morphological profiles, and concatenate spectral and spatial features in a stacked architecture for classification [10, 11].

Despite their simplicity, the feature fusion methods that simply concatenate several kinds of features together are rarely useful in practice. These simple stacking methods can perform even worse than using a single feature, because the information contained by different features is not equally represented or measured. The element values of different features can be significantly unbalanced. Furthermore, the data obtained by stacking several kinds of features may contain redundant information. Last, but not least, the increase in the dimensionality of the stacked features, as well as the limited number of labeled samples in many real applications may pose the problem of the curse of dimensionality and, as a consequence, result in the risk of overfitting the training data.

In this paper, we present our methodology for graph-based fusion of spectral and spatial information, abbreviated

This work was supported by the FWO (Fund for Scientific Research in Flanders) project G037115N "Data fusion for image analysis in remote sensing."

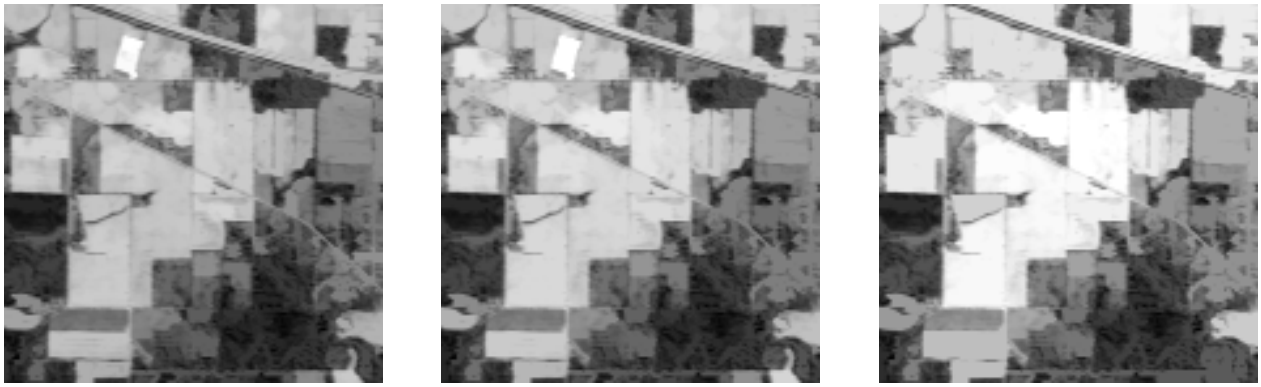

Fig. 1: Morphological opening profile built on the first PC of hyperspectral image. The scale of circular SE varies from 2 to 6, with step size increment of 2. As the size of the SE increases in openings, more small bright objects disappear in the dark background.

by GFSS, and the we give a unifying view on various possible application scenarios. GFSS couples dimension reduction and data fusion of spectral features (from the original HS image) and spatial features contained in the morphological features (computed from the HS image). Variants of this method were very successful in Data Fusion Contests of the IEEE Geoscience and Remote Sensing Society (GRSS) in 2013[1], focusing on the fusion of hyperspectral and LiDAR (Light Detection And Ranging) data [15, 16] and in 2014, focusing on the fusion of thermal hyperspectral and visible images [17]. Here we present the essence of GFSS in a comprehensive way and we focus on fusing the multiple feature sources as a prerequisite for classification. We evaluate the performance of GFSS in combination with support vector machines (SVM) classifier in a case study on an AVIRIS hyperspectral data set, and on a multi-sensor data set (hyperspectral and LiDAR). The organization of this paper is as follows. Section 2 provides a brief review of morphological features. In Section 3, we present our graph-based feature fusion method. The experimental results on real urban hyperspectral images are presented and discussed in Section 4. Finally, the conclusions of the paper are drawn in Section 5.

2. MORPHOLOGICAL FEATURES

Morphological features are generated by either applying morphological openings or closings by reconstruction [2] on the image, using a structural element (SE) of predefined size and shape. An opening acts on bright objects compared with their surrounding, while closings act on dark objects. For example, an opening deletes those bright objects that are smaller than the SE (this means the pixels in the object take on the value of their surrounding). By increasing the size of the SE and repeating the previous operation, a complete morphological profile (MP) is built, carrying information about the size and the shape of objects in the image.

A morphological profile (MP) consists of the opening profile (OP) and the closing profile (CP). For the panchromatic image, MP is built on the original single band image directly. The OP with M scales at pixel $\mathbf{x}$ forms M-dimensional vector, and so does the CP. By incorporating the OP, the CP and original image, the morphological profile of pixel $\mathbf{x}$ is defined as $(2M+1)$-dimensional vector. When applying MP to the hyperspectral data, principal component analysis (PCA) is widely used as a pre-processing step to reduce the dimensionality of the high-dimensional original data, as well as to reduce the redundancy within the bands. Then one applies morphological openings and closings with reconstruction to construct morphological profile on each PC independently. An extended MP (EMP) is formed as a stacked vector consisting of all the morphological profiles. Suppose p PCs are extracted from the original hyperspectral data, then the EMP of pixel $\mathbf{x}$ is a $p(2M+1)$-dimensional vector. Fig. 1 shows a OP built on the first PC. The effect of using morphological features for classification of remote sensing data from urban areas has been discussed in numerous studies [2–5, 8–11].

3. THE GRAPH-BASED FUSION METHOD

Suppose we have multiple feature sources that provide different type of information about the objects on the ground, such that m different attributes $\{Atr_1, \cdots, Atr_m\}$ are available. $\mathbf{X}^{Atr_1} = \{\mathbf{x}_i^{Atr_1}\}_{i=1}^n, \cdots \mathbf{X}^{Atr_m} = \{\mathbf{x}_i^{Atr_m}\}_{i=1}^n$ denote the different attributes after normalization to the same dimension, where $\mathbf{x}_i^{Atr_1} \in \mathbb{R}^D, \cdots, \mathbf{x}_i^{Atr_m} \in \mathbb{R}^D$. $\mathbf{X}^{Sta} = \{\mathbf{x}_i^{Sta}\}_{i=1}^n = [\mathbf{X}^{Atr_1}; \cdots; \mathbf{X}^{Atr_m}] \in \mathbb{R}^{mD}$ denotes the vector stacked by all feature sources. For example, $\mathbf{X}^{Sta} = \{\mathbf{x}_i^{Sta}\}_{i=1}^n = [\mathbf{X}^{Spe}; \mathbf{X}^{Spa}]$, and $\mathbf{x}_i^{Sta} = [\mathbf{x}_i^{Spe}; \mathbf{x}_i^{Spa}] \in \mathbb{R}^{2D}$ denotes stacked spectral and spatial feature sources for HS data, while for HS and LiDAR data, $\mathbf{X}^{Sta} = \{\mathbf{x}_i^{Sta}\}_{i=1}^n = [\mathbf{X}^{Spe}; \mathbf{X}^{Spa}; \mathbf{X}^{Ele}]$, and $\mathbf{x}_i^{Sta} = [\mathbf{x}_i^{Spe}; \mathbf{x}_i^{Spa}; \mathbf{x}_i^{Ele}] \in \mathbb{R}^{3D}$.

[1] $http://hyperspectral.ee.uh.edu/?page\_id = 795$.

$\{\mathbf{z}_i\}_{i=1}^n$, and $\mathbf{z}_i \in \mathbb{R}^d$ denote the fusion features in a lower dimensional feature space with $d \leq mD$.

We aim at finding a transformation matrix $\mathbf{W}$, which can couple dimensionality reduction and feature fusion in a way of:

$$\mathbf{z}_i = \mathbf{W}^T \mathbf{x}_i \tag{1}$$

where $\mathbf{x}_i$ is a variable, which can be set to be $\mathbf{x}_i^{Sta}$. The transformation matrix $\mathbf{W}$ should not only fuse different feature sources in a lower dimensional feature space, but should also preserve local neighborhood information and detect the manifold embedded in the high-dimensional feature space. A reasonable way to find the transformation matrix $\mathbf{W}$ is [12]:

$$\arg\min_{\mathbf{W}} (\sum_{i,j=1}^{n} ||\mathbf{W}^T \mathbf{x}_i - \mathbf{W}^T \mathbf{x}_j||^2 A_{ij}) \tag{2}$$

where the matrix $\mathbf{A}$ is the edge of the graph $\mathbf{G} = (\mathbf{X}, \mathbf{A})$. We assume that the edge (between data point $\mathbf{x}_i$ and $\mathbf{x}_j$) $A_{ij} \in \{0, 1\}$; $A_{ij} = 1$ if $\mathbf{x}_i$ and $\mathbf{x}_j$ are "close" and $A_{ij} = 0$ if $\mathbf{x}_i$ and $\mathbf{x}_j$ are "far apart". The "close" here is defined by finding the k nearest neighbors (kNN) of the data point $\mathbf{x}_i$. The kNN is determined first by calculating a distance between data point $\mathbf{x}_i$ and all the data points, then sorting the distance and determining nearest neighbors based on the k-th minimum distance (we use the Euclidean distance here).

When the graph is constructed by spectral features (i.e. $\mathbf{G} = \mathbf{G}^{Spe} = (\mathbf{X}^{Spe}, \mathbf{A}^{Spe})$), the k nearest neighbors (i.e. $A_{i,j} = A_{i,j}^{Spe} = 1$, $j \in \{1, 2, \cdots, k\}$) of the data point $\mathbf{x}_i^{Spe}$ indicate that the spectral signatures of these kNN data points $\mathbf{x}_j^{Spe}$ are more similar in terms of the Euclidean distance. Similarly, when the graph is constructed by spatial or elevation features (i.e. $\mathbf{G} = \mathbf{G}^{Spa} = (\mathbf{X}^{Spa}, \mathbf{A}^{Spa})$ or $\mathbf{G} = \mathbf{G}^{Ele} = (\mathbf{X}^{Ele}, \mathbf{A}^{Ele})$), the k nearest neighbors (i.e. $A_{i,j} = A_{i,j}^{Spa} = 1$, $j \in \{1, 2, \cdots, k\}$) of the data point $\mathbf{x}_i^{Spa}$ mean that they are more similar in terms of the spatial or elevation characteristics. Let us define a fusion graph $\mathbf{G}^{Fus} = (\mathbf{X}^{Sta}, \mathbf{A}^{Fus})$ as follows:

$$\mathbf{A}^{Fus} = \mathbf{A}^{Atr_1} \odot \mathbf{A}^{Atr_2} \odot \cdots \odot \mathbf{A}^{Atr_m} \tag{3}$$

where the operator '$\odot$' denotes element-wise multiplication, i.e. $A_{i,j}^{Fus} = A_{i,j}^{Atr_1} \cdots A_{i,j}^{Atr_m}$. Note that $A_{ij}^{Fus} = 1$ only if all $A_{ij}^{Atr_1} = 1, \cdots, A_{ij}^{Atr_m} = 1$. This means that the stacked data point $\mathbf{x}_i^{Sta}$ is "close" to $\mathbf{x}_j^{Sta}$ only if their individual feature points $\mathbf{x}_i^{Ind}$ ($Ind \in Atr_1, \cdots, Atr_m$) are "close" to $\mathbf{x}_j^{Ind}$. The connected data points $\mathbf{x}_i^{Sta}$ and $\mathbf{x}_j^{Sta}$ have similar characteristics on all attributes. If any individual feature point $\mathbf{x}_i^{Ind}$ is "far apart" from $\mathbf{x}_j^{Ind}$, then $A_{ij}^{Fus} = 0$. In real data (e.g., HS data), the data points from the roofs ($\mathbf{x}_i^{Sta}$) and roads ($\mathbf{x}_j^{Sta}$) are both made with the same materials (e.g. asphalt) and have similar spectral characteristics ($\mathbf{A}_{i,j}^{Spe} = 1$), but different spatial information (i.e. shape and size) ($\mathbf{A}_{i,j}^{Spa} = 0$), so these two data points are not "close" (i.e. $\mathbf{A}_{i,j}^{Fus} = 0$). On the other hand, the data points from the grassy areas ($\mathbf{x}_i^{Sta}$) and soil areas ($\mathbf{x}_j^{Sta}$) have different spectral characteristics ($\mathbf{A}_{i,j}^{Spe} = 0$), but similar spatial information ($\mathbf{A}_{i,j}^{Spa} = 1$), so $\mathbf{A}_{i,j}^{Fus} = 0$ and these two data points are "far apart". When using the constraint in [13] for avoiding degeneracy:

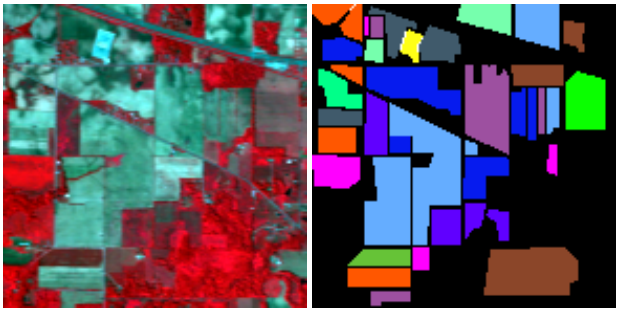

Fig. 2: HSI data sets used in our experiments. Left: false color image of *Indian Pines*; Right: ground truth of the area with 13 classes.

$$\mathbf{W}^T (\mathbf{X}^{Sta}) \mathbf{D}^{Fus} (\mathbf{X}^{Sta})^T \mathbf{W} = \mathbf{I} \tag{4}$$

where $\mathbf{D}^{Fus}$ is a diagonal matrix with $D_{i,i}^{Fus} = \sum_{j=1}^{n} A_{i,j}^{Fus}$ and $\mathbf{I}$ the identity matrix, we can obtain the transformation matrix $\mathbf{W} = (\mathbf{w}_1, \mathbf{w}_2, \cdots, \mathbf{w}_r)$ which is made up by r eigenvectors associated with the least r eigenvalues $\lambda_1 \leq \lambda_2 \leq \cdots \leq \lambda_r$ of the following generalized eigenvalue problem:

$$(\mathbf{X}^{Sta}) \mathbf{L}^{Fus} (\mathbf{X}^{Sta})^T \mathbf{w} = \lambda (\mathbf{X}^{Sta}) \mathbf{D}^{Fus} (\mathbf{X}^{Sta})^T \mathbf{w} \tag{5}$$

where $\mathbf{L}^{Fus} = \mathbf{D}^{Fus} - \mathbf{A}^{Fus}$ is the fusion Laplacian matrix.

4. EXPERIMENTAL RESULTS

The first dataset that we used in the experiments was captured by Airborne Visible/Infrared Imaging Spectrometer (AVIRIS) over northwestern Indiana in June 1992, with 220 spectral bands in the wavelength range from 0.4 to 2.5μm and spatial resolution of 20 meters by pixel. The calibrated data are available online (along with detailed ground-truth information) from http://cobweb.ecn.purdue.edu/~biehl/. The whole scene, consisting of the full 145×145 pixels, which contains 13 classes, see Fig. 2. Table 1 shows the number of labeled samples in each class. Note that the color in the cell denotes different classes in the classification maps (Fig. 2).

Another experiment is done on a hyperspectral image and a LiDAR data which were acquired by the NSF-funded Center for Airborne Laser Mapping (NCALM) on June 2012 over the University of Houston campus and the neighboring urban area. The hyperspectral imagery has 144 spectral bands with

Table 1: *Indian Pines* HS data used in the experiments.

Class No.	Class Name	# Samples	Class No.	Class Name	# Samples
1	Corn-notill	1434	2	Corn-min	834
3	Corn	234	4	Grass/Pasture	497
5	Grass/Trees	747	6	Hay-windrowed	489
7	Soybeans-notill	968	8	Soybeans-min	2468
9	Soybeans-clean	614	10	Wheat	212
11	Woods	1294	12	Bldg-Grass-Trees	380
13	Stone-steel towers	95			

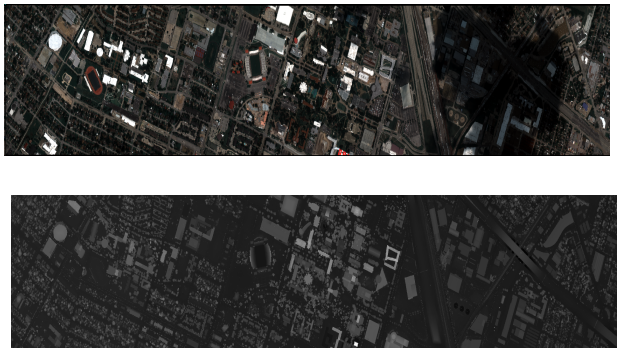

Fig. 3: Multisensor data set: *Houston University*. Top: false color image of hyperspectral image; bottom: LiDAR data.

Table 2: Classification accuracies on *Indian Pines* HS data obtained by different approaches.

	Raw	MPs_{HSI}	Sta	LPP	GFSS
No. of Features	220	83	303	30	36
OA (%)	55.64	83.67	73.01	84.36	**87.27**
AA (%)	65.65	87.82	81.55	87.86	**89.85**
κ	0.506	0.815	0.697	0.823	**0.855**
Corn-notill	40.38	77.75	53.14	76.36	83.33
Corn-min	54.44	93.29	87.53	90.89	**93.17**
Corn	66.67	87.18	87.18	82.05	**90.60**
Grass/Pasture	72.43	77.26	75.86	77.06	**79.07**
Grass/Trees	81.39	92.37	93.17	97.99	**98.26**
Hay-windrowed	98.77	99.59	99.59	95.71	**96.73**
Soybeans-notill	52.17	**78.31**	62.60	81.82	83.06
Soybeans-min	34.40	**77.07**	61.10	75.24	82.13
Soybeans-clean	36.97	**76.38**	69.38	71.17	74.59
Wheat	96.23	**99.53**	99.53	99.53	99.53
Woods	79.06	**87.09**	80.60	97.99	93.59
Bldg-Grass-Trees	45.97	**97.89**	92.63	98.42	98.16
Stone-steel towers	94.74	**97.89**	97.89	97.89	95.79

wavelength range from 380 nm to 1050 nm. Both datasets have the same spatial resolution (2.5m). The whole scene of the data, consisting of the full 349 $\times$ 1905 pixels, contains 15 classes. Fig. 3 shows false color image of HS data and the LiDAR image. For more information, see [15].

To apply the morphological profiles to hyperspectral images, principal component analysis (PCA) was first applied to the original hyperspectral data set, and the first k principal components (PCs) were selected (representing 99% of the cumulative variance) to construct the EMP. A circular SE ranging from 1 to 10 with step size increment of 1 was used. 10 openings and closings were computed for each PC, as well as on LiDAR data.

The SVM classifier with radial basis function (RBF) [14] kernels is applied in our experiments. SVM with RBF kernels has two parameters: the penalty factor C and the RBF kernel width γ. We apply a grid-search on C and γ using 5-fold cross-validation to find the best C within the given set $\{10^{-1}, 10^{0}, 10^{1}, 10^{2}, 10^{3}\}$ and the best γ within the given set $\{10^{-3}, 10^{-2}, 10^{-1}, 10^{0}, 10^{1}\}$. We compare our graph-based approach GFSS with the following schemes: (1) Using original HSI (Raw); (2) Using the MPs computed on the first k ($k = 4$ for *Indian Pines*, $k = 2$ for *Houston University*) PCs of the original HSI (MPs_{HSI}) as in [2], or using MPs built in the same way on the LiDAR data (MPs_{LiDAR}); (3) Stacking all spectral features and MPs together (Sta), similar as in [11]; (4) Features fused by using the graph constructed by stacked features $\mathbf{X}^{Sta}$ [13] (LPP). For Indiana Pines hyperspectral data, we select 20 labeled samples per class for training. The classifiers were evaluated against the remaining labeled samples by measuring the Overall Accuracy (OA), the Average Accuracy (AA) and the Kappa coefficient (κ). For multisensor data sets, available training and testing set are given in Table 3. Table 2 and Table 3 show the accuracies obtained from the experiments, and Fig. 4 shows the classification maps.

It can be found that only using single spectral/spatial feature is not enough for a reliable classification. However, the results also show that it is better sometimes to use a single feature source than simply stacking many of them for

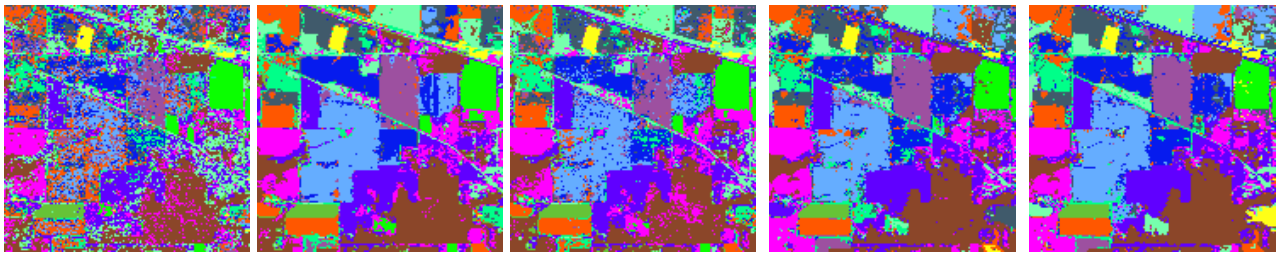

(a) (b) (c) (d) (e)

Fig. 4: Classification maps on *Indian Pines* data produced by the described schemes. Thematic map using (a) original HS data; (b) MPs of HS data; (c) Sta; (d) the LPP; (e) GFSS.

classification. Compared to the situation with single spatial feature (EMP), the OA of simply stacking original spectral and spatial features (Sta) decreases for more than 10 percent, while increasing the dimensionality. This indicates that the spatial information contained by the original EMP was not well exploited in such a stacked architecture. Indeed, when stacking all features together, the element values of different features can be significantly unbalanced, and the information contained by different features is not equally represented. The same problems arise when using the stacked features to build a graph in LPP. For *Indian Pines* hyperspectral data, the graph-based approach GFSS produced the best results, with OA improvements of 4-30% over only using the single spectral/spatial feature source, with improvements of 14% over stacking both the spectral and the spatial features by Sta, and with 3% improvement over the LPP. We have the similar findings for fusion of HS and LiDAR data in *Houston University*, see Table 3.

5. CONCLUSION

In this paper, we give a comprehensive presentation of a graph-based feature fusion method, which enables to include multiple information (e.g., spectral, spatial and elevation) in the classification process. The morphological features, which carry the spatial/elevation information, are first generated on the first few PCs of HS image. Then, we build a fusion graph where only the feature points that are similar in all attributes are connected. Finally, we solve the problem of data fusion by projecting all the features onto a linear subspace. This projection guarantees preservation of the local geometry properties. The neighboring relations are kept after the dimension reduction. Experiments on both real hyperspectral image and multisensor data demonstrate that graph-based fusion method can greatly benefit the accuracy of the subsequent classification.

Acknowledgment

The authors would like to thank Prof. Landgrebe for providing the AVIRIS *Indian Pines* dataset; the Hyperspectral Image Analysis group, and the NSF-Funded Center for Airborne Laser Mapping at the University of Houston for providing the *Houston University* hyperspectral image.

6. REFERENCES

[1] B. C. Kuo and D. A. Landgrebe, "Nonparametric weighted feature extraction for classification", *IEEE Trans. Geosci. Remote Sens.*, vol. 42, no. 5, pp. 1096-1105, May 2004.

[2] J. A. Benediktsson, J. Palmason, and J. R. Sveinsson, "Classification of hyperspectral data from urban areas based on extended morphological profiles", *IEEE Trans. Geosci. Remote Sens.*, vol. 43, no. 3, pp. 480-491, Mar. 2005.

[3] W. Liao, R. Bellens, A. Pižurica, W. Philips and Y. Pi, "Classification of Hyperspectral Data Over Urban Areas Using Directional Morphological Profiles and Semi-Supervised Feature Extraction," *IEEE Journal of Selected Topics in Applied Earth Observations and Remote Sensing*, vol. 5, no. 4, pp. 1177-1190, Aug. 2012.

[4] W. Liao, M. Dalla Mura, J. Chanussot, A. Pižurica, Fusion of Spectral and Spatial Information for Classification of Hyperspectral Remote Sensed Imagery by Local Graph, *IEEE Journal of Selected Topics in Applied Earth Observations and Remote Sensing*, vol. 9, no. 2, pp. 583-594, Feb. 2016.

[5] M. Dalla Mura, J. A. Benediktsson, B. Waske, and L. Bruzzone, "Extended profiles with morphological attribute filters for the analysis of hyperspectral data," *Int. J. Remote Sens.*, vol. 31, no. 22, pp. 5975-5991, Nov. 2010.

[6] G. Camps-Valls, L. Gomez-Chova, J. Munoz-Mari, J. Vila-Frances, and J. Calpe-Maravilla, "Composite ker-

Table 3: Classification accuracies on Fusion of HS and LiDAR from *Houston University* obtained by the described schemes. Note: (# number of training samples/ # number of test samples).

	Original HSI	MPs_{HSI}	MPs_{LiDAR}	MPs_{HSI}+MPs_{LiDAR}	Sta	LPP	Proposed
No. of Features	144	140	70	210	210	26	26
OA (%)	80.72	82.43	69.39	86.39	87.49	87.81	**90.30**
AA (%)	83.40	84.99	68.42	88.48	88.94	88.88	**91.30**
κ (%)	79.23	81.02	66.79	85.31	86.42	86.80	**89.48**
Grass Healthy (#198 / #1053)	82.15	80.25	35.61	**82.43**	81.10	81.10	73.31
Grass Stressed (#190 / #1064)	81.58	80.64	67.11	82.61	84.87	82.80	**97.84**
Grass Synthetis (#192 / #505)	99.80	**100.00**	79.60	**100.00**	**100.00**	**100.00**	**100.00**
Tree (#188 / #1056)	92.80	84.09	72.92	91.10	95.45	97.73	**97.82**
Soil (#186 / #1056)	97.92	**100.00**	83.52	99.91	99.91	98.77	99.24
Water (#182 / #143)	95.10	95.10	66.43	**100.00**	95.80	95.10	99.30
Residential (#196 / #1072)	76.21	87.31	76.59	80.97	86.94	84.24	**88.15**
Commercial (#191 / #1053)	54.51	45.58	91.45	63.06	59.54	79.20	**96.20**
Road (#193 / #1059)	78.47	91.03	59.21	91.88	90.37	91.41	86.59
Highway (#191 / #1036)	60.04	60.42	64.86	64.67	65.44	61.49	**76.83**
Railway (#181 / #1054)	79.51	87.10	88.24	93.45	**99.24**	92.51	92.41
Parking Lot 1 (#192 / #1041)	82.90	86.84	70.89	97.89	99.33	72.98	85.69
Parking Lot 2 (#184 / #285)	72.63	76.49	55.09	**79.30**	77.19	76	76.49
Tennis Court (#181 / #247)	**100.00**	**100.00**	**100.00**	**100.00**	**100.00**	**100.00**	**100.00**
Running Track (#187 / #473)	97.25	**100.00**	14.80	**100.00**	98.94	97.25	99.58

nels for hyperspectral image classification," *IEEE Geosci. Remote Sens. Lett.*, vol. 3, no. 1, pp. 93-97, Jan. 2006.

[7] M. Fauvel, J. Chanussot, and J. A. Benediktsson, "A spatial-spectral kernel-based approach for the classification of remote-sensing images," *Pattern Recognit.*, vol. 45, no. 1, pp. 381-392, 2012.

[8] M. Fauvel, Y. Tarabalka, J. A. Benediktsson, J. Chanussot, J. C. Tilton, "Advances in Spectral-Spatial Classification of Hyperspectral Images," *Proceedings of the IEEE*, vol. 101, no. 3, pp. 652-675, Mar. 2013.

[9] J. Li, P. R. Marpu, A. Plaza, J. M. Bioucas-Dias and J. A. Benediktsson, "Generalized Composite Kernel Framework for Hyperspectral Image Classification," *IEEE Trans. Geosci. Remote Sens.*, vol. 51, no. 9, pp. 4816-4829, Sep. 2013.

[10] J. A. Palmason, J. A. Benediktsson, J. R. Sveinsson, and J. Chanussot, "Fusion of morphological and spectral information for classification of hyperspectral urban remote sensing data," *in Proc. IGARSS 06*, pp. 2506C2509, Jul. 2006.

[11] M. Fauvel, J. A. Benediktsson, J. Chanussot and J. R. Sveinsson, "Spectral and Spatial Classification of Hyperspectral Data Using SVMs and Morphological Profile", *IEEE Trans. Geosci. Remote Sens.*, vol. 46, no. 11, pp. 3804-3814, Nov. 2008.

[12] M. Belkin and P. Niyogi, "Laplacian Eigenmaps and Spectral Techniques for Embedding and Clustering," *Advances in Neural Information Processing Systems 14*, pp. 585-591, MIT Press, British Columbia, Canada, 2002.

[13] X. F. He, P. Niyogi, "Locality preserving projections," *Advances in Neural Information Processing Systems 16*, pp. 153-160, MIT Press, Cambridge, 2004.

[14] C. C. Chang and C. J. Lin, "LIBSVM: A Library for Support Vector Machines", 2001, *http://www.csie.ntu.edu.tw/ ˜cjlin/libsvm*.

[15] C. Debes, A. Merentitis, R. Heremans, J. Hahn, N. Frangiadakis, T. Kasteren, W. Liao, R. Bellens, A. Pižurica, S. Gautama, W. Philips, S. Prasad, Q. Du, F. Pacifici, "Hyperspectral and LiDAR Data Fusion: Outcome of the 2013 GRSS Data Fusion Contest," *IEEE Journal of Selected Topics in Applied Earth Observations and Remote Sensing*, vol.7, no. 6, pp. 2405-2418, March 2014.

[16] W. Liao, R. Bellens, A. Pižurica, S. Gautama, W. Philips, "Generalized Graph-Based Fusion of Hyperspectral and LiDAR Data Using Morphological Features," *IEEE Geoscience and Remote Sensing Letters*, vol. 12, no. 3, pp. 552-556, Mar. 2015.

[17] W. Liao, X. Huang, F. Coillie, S. Gautama, A. Pižurica, W. Philips, H. Liu, T. Zhu, M. Shimoni, G. Moser, and D. Tuia, "Processing of Multiresolution Thermal Hyperspectral and Digital Color Data: Outcome of the 2014 IEEE GRSS Data Fusion Contest," *IEEE Journal of Selected Topics in Applied Earth Observations and Remote Sensing*, vol. 8, no. 6, pp. 2984-2996, June 2015..